SUPPLEMENTARY MATERIAL

Supplementary Methods

From February to August 2020, 49 kidney transplant recipients older than 18 years were included. Patients were those who were previously referred for ultrasound examination in our adult radiology department at Necker University Hospital. In clinical routine, these subjects receive several postoperative ultrasounds: on day 1, then on month 3, on month 12, and annually. They also receive ultrasound scans in case of graft dysfunction to explore a surgical or medical complication. The examination includes B-mode, classical Dopplers (Color Doppler, Superb Microvascular Imaging, and Advanced Dynamic Flow), and pulsed Doppler acquisitions. An ultrasound acquisition with Sonovue® microbubbles injection (Bracco) is also performed to explore hypo- or avascular areas and necrosis: thus, no additional injection was necessary for this study and we used the same type of acquisition to perform the ULM. In addition, to avoid motion artifacts in the acquisitions, patients were supine and breathing slowly.

We started to optimize the CEUS mode embedded in the clinical scanner on the first 15 patients to have satisfactory ULM images. To perform ULM, we used an Aplio i800 (Canon MS, Nasu, Japan) and an i8CX1 convex abdominal probe (3 MHz). Probes used to perform conventional Doppler techniques were either i8CX1 (3MHz) or i11LX3 (7MHz). The dynamic range and gain were adapted to the ultrasound machine, which allowed better discrimination of microbubbles and facilitated their localization. Because of the superficial position of the renal graft in the iliac fossa, we were able to reduce the imaging depth to explore between 4 and 10 cm, resulting in a maximum clip time of 1 to 3 minutes. In this way, we could increase the frame rate (between 14 and 64Hz). Data were collected in DICOM format and all dynamic clips were stored anonymously on a hard disk. From 2 to 4 clips were stored per patient resulting in a total of 142 clips for the 49 patients. All data analyses were performed at the Biomedical Imaging Laboratory by members of the PPM (Physiology Pathology of the Microcirculation) team, specialist in ULM for over 5 years.

After optimization of the probe's positioning on 5 patients, we searched for time-window with the optimal number of microbubbles on 15 patients. The injection of a bolus of 1.2 mL of microbubbles, followed by an injection of 10 ccs of saline, was repeated twice, as in the clinical routine. The optimal number of microbubbles, i.e. to have isolated ones, was reached during

the late venous phase, i.e. on average between 45 and 192 seconds after injection. The difference in microbubbles concentration between a too-early phase (too many microbubbles), an optimum phase (many distinct microbubbles), and a delayed phase (disappearing microbubbles) was observed in CEUS acquisitions (Supplementary Figures S1). We used a low mechanical index (=0.07) to exploit the non-linear properties of microbubbles [S1] by limiting their destruction. The examination duration then depends almost exclusively on the natural lifetime of the microbubbles in the blood compartment.

In short, from the 49 included KTRs, 35 were used for the optimization of CEUS mode, probe's positioning, and microbubbles optimal number targeting. The remaining 14 were used to perform ULM, and among them, 7 were excluded because of respiratory movements: results on the remaining 7 are presented in this study.

To do ULM images, clips were divided into blocks of 200 frames each: a clip of 173 seconds at 22 Hz corresponding to 3812 consecutive frames was thus divided into 20 blocks. ULM was achieved with classical steps on each block: filtering, localization of microbubbles, tracking, and track accumulation. Filtering was already done by the CEUS mode embedded in the ultrasound system (Supplementary Figures S2a): bandpass filters with cutoff frequencies from 0.5 to 8.5Hz have been added to enhance the moving microbubbles. Localization has been realized thanks to a 2-D Gaussian filter with a standard deviation of 1 pixel (i.e. from 0.07 to 0.17mm) and targeting of the regional maximums (Supplementary Figures S2b). Tracking was performed with the Hungarian algorithm method [S2] using a maximum distance between the microbubbles of 1 to 2.8mm and a minimum track duration varying from 0.08 to 0.4 seconds (Supplementary Figures S2c). Finally, tracks accumulation of the 8 to 35 blocks, allowed us to obtain a vascular density map of the kidney (Supplementary Figures S2d).

We keep the same pixel size for ULM maps as the original grid (from 0.07 to 0.17mm). We measured five vessels' diameters in Doppler modes and ULM with the cross-section technique [S3, S4] (Supplementary Figures S3) in every 7 patients: we thus have an estimation of the mean of these thirty-five vessels' diameters, their standard deviation, and an estimation of the average of the 7 smallest vessels for each technique. The intensity of the red component was used to estimate diameter on ADF, SMI, and color Doppler (color of segmented vessels).

It is important to specify that these measurements are not resolution measurements but measurements of the vessels' diameters, which can give us an idea of the resolution achieved by each of the ultrasound techniques. Pixel size of each ultrasound techniques, also called spatial resolution, have been described in Supplementary Table S1.

Velocity encoding was performed and overlaid on the density map. Directions were encoded in red when tracks go towards the probe, and in blue when they go away from it. To perform a quantitative ULM analysis, we manually segmented the kidney capsule and upper cortex area to investigate a potential correlation between vessel velocity and its distance to the capsule (Supplementary Figures S4). This analysis was performed only on tracks present in the upper cortex for two reasons: the lower kidney capsule was not visible on acquisitions, and to avoid aliasing bias present in the bigger vessel by ULM. Indeed, max speed detected by ULM varies from 2cm/sec to 6cm/sec whereas biggest kidney vessels speed is normally around 100cm/sec [S5].

All image processing was made with MATLAB (Mathworks).

Statistical analyses were performed with Graphpad Prism 9 software. Student's t test was performed to quantify the differences between vessel cross sections with a 95% confidence level. The significance of the results is as follows: ns = $P > 0.05$, * = $P \leq 0.05$, ** = $P \leq 0.01$, *** = $P \leq 0.001$, **** = $P \leq 0.0001$.

SRQR reporting guidelines were applied [S6].

Supplementary Figures

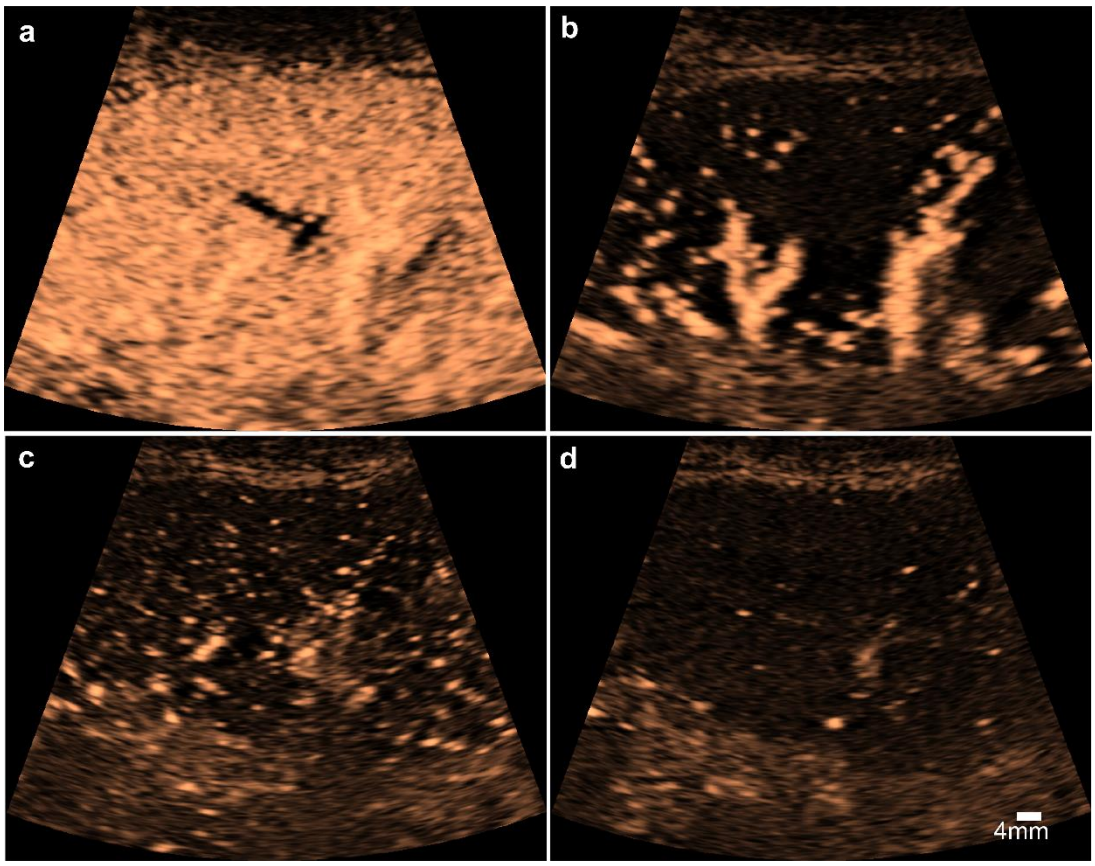

Supplementary Figure. S1. Difference in microbubbles concentration in patient 1. (**a**) Contrast Enhanced Ultrasound acquisitions in clinical practice. (**b**) Microbubbles early arrival. (**c**) Late venous phase (optimal phase). (**d**) Very delayed phase. The colormap comes from the ultrasound scanner without specification (arbitrary unit). The scale bar is the same as in d for all 4 images.

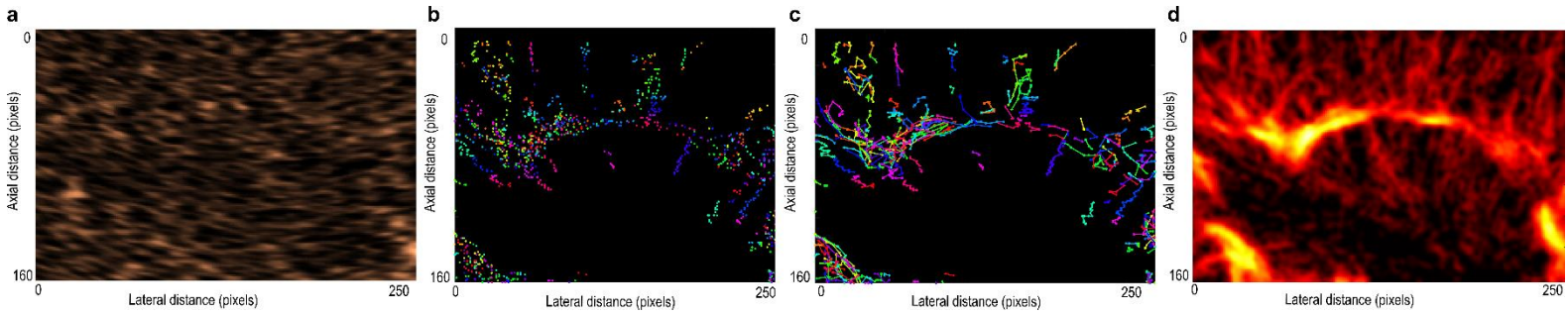

Supplementary Figure.S2. Framework of ULM image formation in zoomed patient 1. (**a**) Contrast Enhanced Ultrasound (CEUS) acquisition with a clutter filter integrated in the clinical echograph. The color map comes from the ultrasound scanner without specification (arbitrary unit). (**b**) Localization of microbubbles thanks to a 2D gaussian filter in one bloc (arbitrary colors). (**c**) Tracking thanks to Hungarian algorithm in the same bloc (arbitrary colors). (**d**) ULM density map resulting from the accumulation of twenty blocs (density colormap from 0 to 4.5 in arbitrary units).

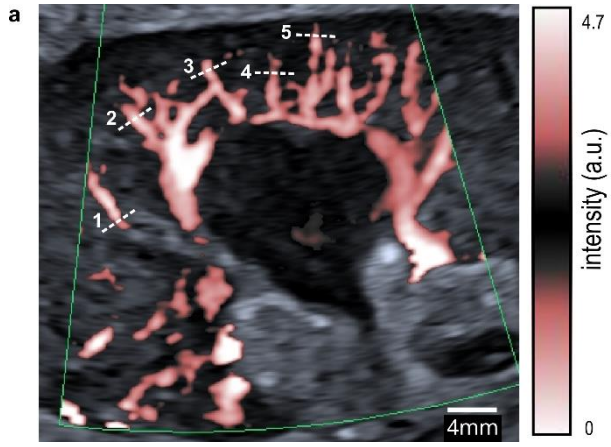

Supplementary Figure.S3. Example of cross-section measurement in Superb Microvascular Imaging (SMI), with contrast agent, acquisition in patient 1. (**a**) SMI, with contrast agent, image with five cross-sectioned vessels indicated with dotted white lines. The color map comes from the ultrasound scanner without specification (arbitrary unit). (**b**) Diameter measured as the width at half the maximum intensity (of the red component), in the third manually cross-sectioned vessel. Red arrow indicates the width at half the maximum intensity.

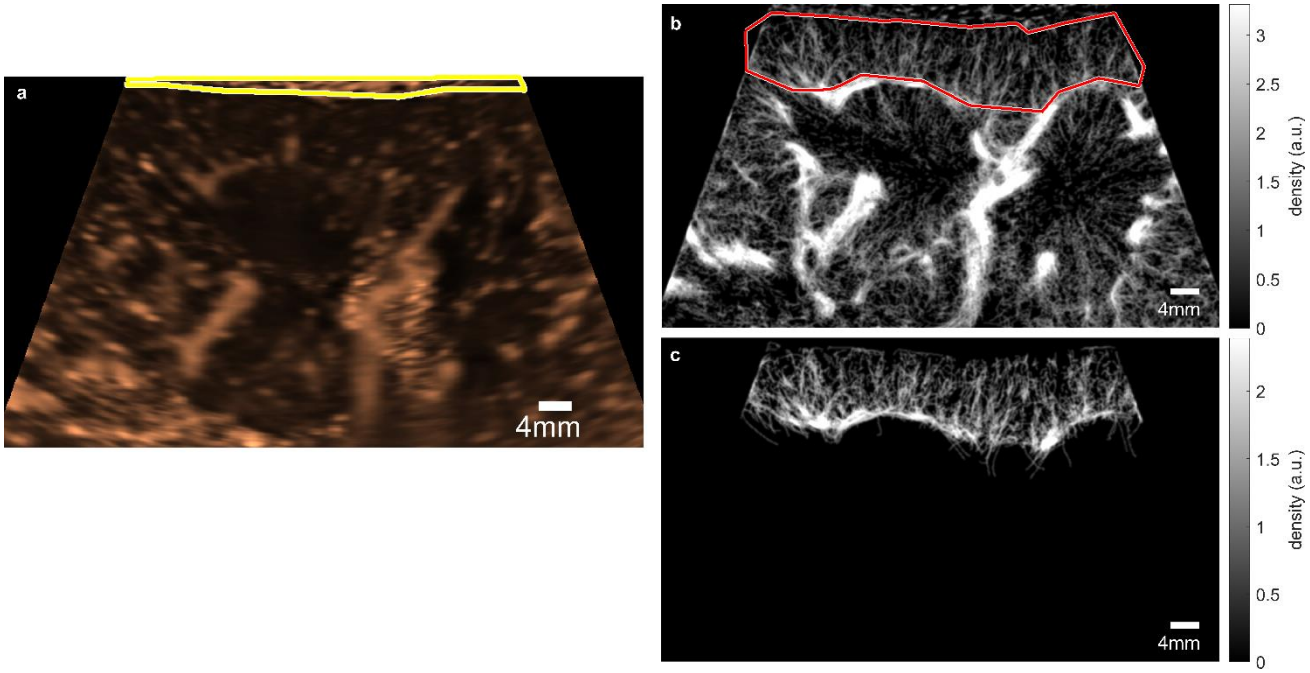

Supplementary Figure.S4. Kidney capsule and upper cortex manual segmentation on patient 1. (**a**) Capsule segmentation made on temporal mean of the first block of CEUS acquisition in patient 1. Kidney capsule is indicated with a yellow line. The color map comes from the ultrasound scanner without specification (arbitrary unit). (**b**) Upper cortex segmentation made on ULM density map. Cortex mask is drawn with a red line. (**c**) Resulting cortex tracks from the upper cortex segmentation. If at least one point of a track was present in the upper cortex mask, track was preserved.

Supplementary Tables

Patients n°	Pixel resolution (mm)			
	CEUS	ADF	SMI	Color Doppler
1	0.12	0.07	0.10	0.07
2	0.07	0.15	0.15	0.18
4	0.12	0.15	0.07	0.18
10	0.14	0.08	0.13	0.15
11	0.17	0.18	0.17	0.17
13	0.15	0.18	0.13	0.17
19	0.10	0.13	0.15	0.13

Supplementary Table S1. Pixel resolution of each ultrasound modes in each patient.

Patient number	Etiology of initial renal failure	Sonovue Dose (mL)	Time frame of the transplantation	Dilation of the pyelo-caliceal cavities	SRT (ms)	RI interlobar arteries	Nb of grefon veins	Nb of grefon arteries	Creatinin (µmol/L)	Graft depth (mm)	BMI (kg/m²)	Age (y)	Sex
1	Cystinosis	1.2	11 days	No	<200	0.72 - 0.82	1	1	105	9	31	33	F
2	Valve of the posterior urethra	1.2	12 hours	No	<200	0.41 - 0.52	1	1	180	15	24	19	M
3	TSB + ADPKD	1.2	3 days	No	<200	0.82 - 0.89	1	2	203	36	25	36	F
4	MPGN	1.2	17 days	No	<200	0.62 - 0.65	1	1	130	24	21	19	M
5	Diabetic nephropathy	1.2	24 hours	No	<200	0.76 - 0.92	1	2	111	27	28	55	M
6	Nephropathy indeterminate	1.2	6 months 3 days	No	<200	0.67 - 0.72	1	2	200	14	32	28	M
7	Berger's disease	1.2	10.5 years	No	<200	0.75 - 0.85	1	1	380	15	29	68	M

86

Supplementary Table S2. Patient characteristics.

TSB: Tuberous sclerosis of Bourneville; ADPKA: Autosomal Dominant Polycystic Kidney Disease; IR: Resistance Index; SRT: Systolic Rise Time; MPGN: Membranoproliferative glomerulonephritis.

Supplementary References

S1. Brown J, Christensen-Jeffries K, Harput S, et al. Investigation of Microbubble Detection Methods for Super-Resolution Imaging of Microvasculature. *IEEE Trans Ultrason Ferroelectr Freq Control*. 2019;66(4):676-691. doi:10.1109/TUFFC.2019.2894755

S2. Tinevez JY, Perry N, Schindelin J, et al. TrackMate: An open and extensible platform for single-particle tracking. *Methods*. 2017;115:80-90. doi:10.1016/j.ymeth.2016.09.016

S3. Errico C, Pierre J, Pezet S, et al. Ultrafast ultrasound localization microscopy for deep super-resolution vascular imaging. *Nature*. 2015;527(7579):499-502. doi:10.1038/nature16066

S4. Hingot V, Errico C, Heiles B, et al. Microvascular flow dictates the compromise between spatial resolution and acquisition time in Ultrasound Localization Microscopy. *Sci Rep*. 2019;9(1):2456. doi:10.1038/s41598-018-38349-x

S5. Pellerito J, Polak J. Introduction to Vascular Ultrasonography. *Elsevier Health* Sciences; 2019.

S6. O'Brien BC, Harris IB, Beckman TJ, et al. Standards for reporting qualitative research: a synthesis of recommendations. *Acad Med.* 2014;89(9):1245-1251.